Peer Reviewed Paper openaccess

Hyperspectral image non-linear unmixing using joint extrinsic and intrinsic priors with $L_{1/2}$-norms to non-negative matrix factorisation

K. Priya* and K.K. Rajkumar

Kannur University, Thavakkara, Civil Station PO, Kannur, India

Contact
K. Priya: kodothpriya@gmail.com K. Rajkumar: rajatholy@yahoo.in

Hyperspectral unmixing (HU) is one of the most active emerging areas in image processing that estimates the hyperspectral image's endmember and abundance. HU enhances the quality of both spectral and spatial dimensions of the image by modifying the endmember and abundance parameters of the hyperspectral images. There are several HU algorithms available in the literature based on the linear mixing model (LMM) that deals with the microscopic contents of the pixels in the images. Non-negative matrix factorisation (NMF) is the prominent method widely used in LMMs that simultaneously estimates both the endmembers and abundances parameters along with some residual factors of the image to improve the quality of unmixing. In addition to this, the quality of the image is enhanced by incorporating some constraints to both endmember and abundance matrices with the NMF method. However, all the existing methods apply any of these constraints to the endmember and abundance matrices by considering the linearity features of the images. In this paper, we propose an unmixing model called joint extrinsic and intrinsic priors with $L_{1/2}$ norms to non-negative matrix factorisation (JEIp $L_{1/2}$-NMF) that applies multiple constraints simultaneously to both endmember and abundance matrices of the hyperspectral image to enhance its quality. Three main external and internal constraints such as minimum volume, sparsity and total variation are applied to both the endmembers and abundance parameters of the image. In addition, a $L_{1/2}$-norms is imposed to extract good quality spectral data. Therefore, the proposed method enhances spatial as well as spectral data and considers the non-linearity of the pixels in the image by adding a residual term to the model. Performance of our proposed model is measured by using different quality measuring indexes on four benchmark public datasets and found that the proposed method shows outstanding performance compared to all the conventional baseline methods. Further, we also evaluated the performance of our method by varying the number of endmembers empirically and concluded that less than five endmembers provides high-quality spectral and spatial data during the unmixing process.

Keywords: hyperspectral unmixing, JEIp $L_{1/2}$-NMF, minimum volume, non-linear mixing model (NLMM), non-negative matrix factorisation (NMF), sparsity, total variation

Correspondence
K. Priya (kodothpriya@gmail.com)

Received: 10 November 2021
Revised: 24 December 2021
Accepted: 24 February 2022
Publication: 7 April 2022
doi: 10.1255/jsi.2022.a4
ISSN: 2040-4565

Citation
K. Priya and K.K. Rajkumar, "Hyperspectral image non-linear unmixing using joint extrinsic and intrinsic priors with $L_{1/2}$-norms to non-negative matrix factorisation", *J. Spectral Imaging* **11,** a4 (2022).
https://doi.org/10.1255/jsi.2022.a4

Introduction

Hyperspectral imaging (HSI) captures a contiguous spectrum of wavelengths over a selected range of intervals for each pixel in the image. This feature increases the hyperspectral image with many more spectral bands compared to conventional imaging technology. The high spectral resolution of HSI strengthens its information storing ability which provides the mechanism for analysing the different characteristics of the materials present in the image at the pixel level of the captured image. This characteristic of hyperspectral images makes this imaging model well suited to various applications like object identification, medical diagnosis, pattern recognition, remote sensing, agriculture, food safety etc. Each spectral band in hyperspectral images is divided into a narrow wavelength range, therefore, the amount of the energy collected by hyperspectral sensors per unit time is limited. Due to this narrow division of spectral bands in HSI, it is easily affected by noise during the time of acquisition. This may lead to reduction in the spectral and spatial quality of HSI. Nowadays, many algorithms have been introduced to improve the spectral and spatial quality of HSI. One way is to fuse the high spectral quality of HSI with high spatial quality images like RGB or multispectral imaging (MSI). The fusion between MSI and HSI gives better spatial quality for HSI because spectral correlation with these two images is high compared to conventional imaging modalities. From the literature, it seems that spectral unmixing based image fusion is an emerging, and one of the most effective, methods for enhancing spatial quality of HSI due to its complex structure of the images which contain multiple spectral bands.[1]

In HSI, each pixel in the images is a mixture of several kinds of materials of the scene and it is represented in a complex structure. Due to this complex structure, it is, practically, a challenging task to analyse in-depth or detailed hyperspectral images using conventional imaging systems. However, each spectral band in the hyperspectral images is divided into a narrow wavelength range, therefore, the number of photons influenced on the sensor per unit time is limited. This fact makes it impossible to acquire a high spatial resolution hyperspectral image both in space and time. Due to this lower resolution in the spatial data, each pixel in the hyperspectral image may be composed of several kinds of materials in the scene, called mixed pixel. This mixed pixel problem has a serious affect in the quantitative development of the spectral imaging field and also in various applications of computer technology. Therefore, it is necessary to identify and calculate the proportion of each spectral component present in the mixed pixels. This process of separating each mixed pixel is called spectral unmixing. Therefore, hyperspectral unmixing (HU) has been introduced to overcome this limitation. HU can be effectively utilised for analysing minute details of the pixel in the image. This method consists of three steps: selecting the desired number of endmembers from the scene, extracting spectral signatures of the selected endmembers and finally estimating the fractional abundances of these endmembers. The first spectral unmixing method is pansharpening. The pansharpening method includes a pixel-wise fusion between the spatial data of panchromatic (PAN) images with spectral data of multispectral images. The pansharpening methods are also extended for the fusion of hyperspectral and PAN images with the increasing availability of hyperspectral images. This hyperspectral-pansharpening causes some limitations during the fusion process due to the spectral trade-off between HSI and pansharpening. The hyperspectral-multispectral fusion method was introduced later. In hyperspectral-multispectral spectral unmixing based fusion, the unmixing process is applied on both hyperspectral images and multispectral images and then fuses the necessary data from these images. That means fusing high spectral resolution from hyperspectral images and high spatial information from multispectral images to reconstruct a high-quality hyperspectral image.

The spectral unmixing (SU) algorithm can be characterised into two mixing models, namely the linear mixing model (LMM) and the non-linear mixing model (NLMM). These mixing models show how the materials in each pixel interact with each other and reflect when light falls on it to form the spectral signature. An analysis of the literature reveals that most of the existing baseline unmixing algorithms are based on the LMM. LMM considers only the macroscopic scale of mixing that estimate endmembers, and their fractions abundance based on the single level reflection of light on each pixel in the hyperspectral image. The NLMM considers the microscopic level of interaction, i.e it considers the multiple reflection of materials in the pixels, but requires a complex algorithm and more computational time. This complex information obtained from NLMMs is not necessary in many real-life situations and may sometimes give inconsistent results due to the over-fitting nature of the data. In such a case, the simple LMM becomes more convenient model for analysing the multispectral pixel information in the image.[2]

Recently, many LMM-based unmixing algorithms have been used to consider the basic non-linearity information of the pixels in the image. In this paper, we propose a non-negative matrix factorisation (NMF)-based LMM method for extracting the non-linear effects of the pixels in the image. The proposed method is built on the standard LMM with some regularisation parameters, viz. minimum volume (MV), total variation (TV) and sparsity constraints to both spectral and spatial features of the pixel information to accommodate the non-linear effects of the image.

NMF is an attractive and widely used model for the HU process.[3] But in the NMF model, many minimum solutions occur locally due to its non-convexity nature. A non-convex optimisation problem has multiple feasible or minimum solutions. These multiple local minima make it a challenge to obtain a finite optimal solution of the NMF problem. Therefore, adding the abundance sum-to-one constraint (ASC) and abundance non-negative constraint (ANC) into the NMF solution space helps to alleviate the non-convexity situation. The ASC normalises the range of pixels in the image to unity and ensures the data distribution is equal in each pixel of the image. Similarly, the ANC reduces the complexity and provides faster convergence to the problem. To further shrink the solution space of the NMF model, it is necessary to add some more constraints to the spectral and spatial quality of the image.[4]

Recently, a number of papers have proposed constrained NMF by incorporating some additive terms to the original NMF-based LMM. But most of these existing NMF-based unmixing algorithms impose constraints on any one of the two matrices, namely in the endmember matrix or the abundance matrix. Imposing such constraints in only one matrix may cause some limitations in the quality of the unmixing process. Therefore, to improve the effectiveness and accuracy of the NMF-based unmixing algorithm, in this paper we propose a model by adding constraints to both of the NMF matrices, such as endmember and abundance matrices.[5]

In this paper we introduce a new blind unmixing method called joint extrinsic and intrinsic priors with $L_{1/2}$ norms to non-negative matrix factorisation (JEIp $L_{1/2}$-NMF) to both the endmember and abundance matrices of the NMF model. The extrinsic priors of the hyperspectral image are based on the geometrical and intrinsic prior-based statistical framework of the image. By imposing these two constraints or priors to the NMF model, ultimately we aim to enhance the quality of the hyperspectral image's spectral as well as spatial data. In addition, we use $L_{1/2}$ regularisation to the NMF method which provides sparse-based unmixing and yields a more accurate estimation of spatial data.

The geometrical unmixing extracts endmember or pure pixels present in the spectral information of the hyperspectral image. This spectral information is acquired from the vertices of a simplex. A simplex is a minimum possible hypercube formed from the image's data points called endmembers. This endmember determines the volume of the simplex, which is one of the essential prior considerations in spectral image analysis. To control the structural information and improve the unmixing performance, choosing the simplex with MV is necessary. The centroid-based MV regulariser controls the distance between centre point and endmember vertex. This makes the selected endmember closer to the centre point of the simplex denoted by μ.[6]

In statistical SU, each pixel of the hyperspectral image is decomposed as a linear combination of pure endmember spectra. The estimation of pure endmember spectra is based on the posterior distribution of abundances and endmember parameters under a hierarchical Bayesian model.[4] The statistical information depends on the abundance or spatial quality of the image. In general, abundance sparsity and smoothness are typical constraints applied on spatial data of the spectral images. In addition to this, our paper also addresses the non-linearity effects and $L_{1/2}$-norms in the spatial data which helps to remove the zero value to a large extent. The non-linear effects account for the residual noise, spectral and spatial variability occurring in the specific locations of the image. These non-linear effects are named as outlier residual terms in the image.[7]

Related work

Recent works in the literature proposed many LMM unmixing algorithms by using NMF concepts. Lina Zhuang *et al.*[6] proposed a non-negative matrix factorisation-quadratic minimum volume-based (NMF-QMV) in which they imposed a MV constraint to the unmixing algorithm. These MV constraints minimise the volume of simplex formed from the columns of endmember matrices by reducing the non-convexity problem and computational complexity during the optimisation process.

Yuan *et al.*[8] proposed a hyperspectral image unmixing method named an improved collaborative non-negative matrix factorisation and total variation (ICoNMF-TV) algorithm to enhance the quality of the hyperspectral image. In this method, the authors introduced a total

variation (TV) regulariser for the abundance matrix to provide piecewise smoothness between adjacent pixels. This TV is calculated by computing the difference between adjacent pixels in horizontal and vertical directions. Therefore, this unmixing method enhances the spatial quality and promotes the performance and efficiency of the HU algorithm.

Lei Zhou *et al.*[9] proposed an NMF unmixing method based on spatial information by considering the original image into subspace structure which helps to capture detailed distribution of spatial information. This subspace structure helps to identify the globally distributed materials on different parts of the image. Finally, this method incorporates the sparse-NMF framework to consider the amount of sparsity in the abundance matrix. Therefore, this method improved the spatial quality as well as the performance of the unmixing algorithm.

Wei He *et al.*[10] introduced a total variation regularised reweighted sparse-NMF (TV-RSNMF) unmixing method. This method incorporates a reweighted sparse unmixing method which encourages more abundance map sparsity than the existing L_1 norm method. In addition to this, the TV regulariser is also embedded into this method to provide spatial smoothness to the image. Thus TV-RSNMF provides piecewise smoothness and denoising to the abundance map of the hyperspectral image and hence our proposed method JEIp $L_{1/2}$-NMF improves the visual quality to the hyperspectral image to a great extent.

Kewen Qu *et al.*[11] proposed an unmixing algorithm, namely multiple-priors ensemble constrained NMF (MPEC-NMF). In this work, the NMF unmixing method combines both the geometrical and statistical prior of the hyperspectral image. The endmember matrix is imposed with MV constraints to strengthen spectral data quality using geometric prior. The statistical prior imposes TV constraints to provide a spatial smoothness and the sparsity constraints to account for the number of zero or null values in the abundance map. These two statistical priors are the most significant constraints applied to the abundance matrix. Thus, the MPEC-NMF method incorporated all the essential constraints that enhance the spatial as well as spectral data of the hyperspectral image. But all these methods did not consider the non-linearity effects in the image. So, it is challenging to consider specific or localised areas such as the edges, the boundary of heterogeneous regions in the hyperspectral images.

Due to the simplicity of the LMM method, most of the existing unmixing algorithms use LMM-based NMF for the HU process. Moreover, the LMM-based NMF unmixing method provides a good approximation in many fundamental observations of the image. This behaviour makes the LMM a helpful technique for many applications. But all these existing LMM-based unmixing algorithms available in the literature do not consider the fundamental non-linearity in the image. In some situations, such as sand-like scenes, incident light scattered and absorbed through multiple materials present in each pixel in the image may result in a non-linear effect. In such a situation, LMM may be inaccurate in handling the unmixing due to the non-linearity or outlier effects in the image. Therefore, it is necessary to consider the non-linear mixing concept during the HU process.[7] So, the method that we are going to propose in this paper introduces a NMF-based LMM method by incorporating the non-linear effects described by adding some additional constraints to both the endmember and abundance parameters of a conventional linear mixing model. The proposed method builds on the standard LMM, with some regularisation terms that enhance the accuracy of both spectral and spatial dimensions makes non-linear effects in the HU.

Dataset

In order to evaluate the efficiency and effectiveness of our proposed algorithm, we used four different hyperspectral data sets available online. The first dataset is the Washington DC Mall, a well-known dataset captured by the HYDICE sensor. This dataset contains an image of size 1278 × 307 pixels with 191 spectral bands with 0.4–2.5 μm spectral range. Due to the large size of the image, we cropped it into a 240 × 240 pixels for our experiment.[12] The second dataset is NEON Data, and this provides information on the National Observatory Networks San Joaquin Experimental Range field site. This image was collected over the San Joaquin field site located in California. The image selected for this experiment consists of 500 × 500 pixels with 107 bands with 0.4–0.85 μm spectral range.[13] The third hyperspectral dataset is Pavia University captured by the reflective optics spectrographic imaging system (ROSIS-3) over the University of Pavia, northern Italy, in 2003. It consists of 610 × 340 pixels with 103 bands with 0.430–0.838 μm spectral range. The image is cropped into 560 × 320-pixel size for our experiment.[14] Finally, the fourth hyperspectral image dataset, AVIRIS Indian Pines, was captured by the AVIRIS sensor over the Indian Pines test site in northwestern Indiana, USA, in 1992. The image consists of

512 × 614 pixels. The image selected for our experiment is cropped into 350 × 360-pixel size and 192 bands with wavelength ranges from 0.4 µm to 2.5 µm.[15]

Quality measures

The quality of hyperspectral images after various unmixing algorithms has been estimated based on endmember and abundance estimation accuracy using various performance matrices presently available in the literature. The most commonly used such quality measures are spectral angle mapper (SAM), signal-to-reconstruction error (SRE), root-mean-square error (RMSE), peak signal-to-noise ratio (PSNR) and universal image quality index (UIQI). These five quality measures are used to determine the performance quality of our proposed JEIp $L_{1/2}$-NMF algorithm.[15]

Spectral angle mapper (SAM)

SAM identifies the spectral distortion between the estimated spectra E and a ground truth spectrum $\hat{E}$ with n number of pixels. It measures the spectral similarity between the estimated and reference spectra by calculating the angle difference of the vectors between them as follows:

$$\mathrm{SAM}\left(E,\hat{E}\right) = \frac{1}{n}\sum_{j=1}^{n}\arccos\left[\frac{E_j^T \bullet \widehat{E_j}}{E_{j2} \bullet \widehat{E_{j2}}}\right] \tag{1}$$

The arccosine defines the inverse cosine function of the given value. If higher, the spectral similarity between estimated spectra E and a ground truth spectrum $\hat{E}$ SAM values are closer to zero. That means a SAM value near to zero indicates high spectral quality.[16]

Signal-to-reconstruction error (SRE)

The SRE measures the quality of the reconstructed image based on the accuracy of the estimated abundance data in the image. Using this parameter, we can decide the quality of the image as well as the efficiency of the proposed algorithm. The SRE is measured as follows,

$$SRE = 10\log_{10}\left(\frac{\frac{1}{n}\sum_{i=1}^{n}\hat{A}_{i2}^2}{\frac{1}{n}\sum_{i=1}^{n}\hat{A}_i - A_{i2}^2}\right) \tag{2}$$

where the number of pixels denoted by n, and $\hat{A}_i$ and A_i denote the abundance vectors of the estimated and original image at the ith pixel. The larger the SRE value, the higher the spatial quality of the image.[5]

Root-mean-square error (RMSE)

The RMSE calculates the average difference between the original and estimated abundance map of the image. Therefore, the RMSE value gives the quality of unmixing algorithm and the reconstructed image. That means this matrix measures the spatial quality between the reference abundance $\hat{A}$ and estimates abundance image A which is defined as:

$$\mathrm{RMSE}(\hat{A},A) = \frac{1}{\lambda_h n_m} A - \hat{A}_F^2 \tag{3}$$

where λ_h and n_m are the number of bands and the pixels in each of the bands. A and $\hat{A}$ represents the referenced and estimated abundance image. The ideal value of RMSE is equal to zero, and it can be achieved when $\hat{A} = A$, which indicates that there is no deviation. A smaller RMSE value indicates that better quality of the image.[17]

Peak signal-to-noise ratio (PSNR)

The PSNR value gives the quality of the spatial data in the reconstructed image in band-wise. In general, PSNR value is measured as the ratio between the signals to the residual errors. The PSNR of the lth band can be defined as:

$$\mathrm{PSNR} = \frac{1}{\lambda_h}\sum_{l=1}^{\lambda_h}\mathrm{PSNR}_l \tag{4}$$

where PSNR_l measures the spatial quality in the lth spectral band is defined as:

$$\mathrm{PSNR}_l = 10 \bullet \log_{10}\left(\frac{\max\left(A^l\right)^2}{\widehat{A^l} - A^l / P}\right) \tag{5}$$

where A^l is the pixel value of the lth abundance band in the image. The higher the PSNR value, the better the spatial quality of the estimated image.[18]

Universal image quality index (UIQI)

UIQI measures the similarity between the original and the estimated images. This is done by calculating the average correlation between both images. If Y_i denotes the original image at the ith band and $\widehat{Y}_i$ denotes the estimated image at the corresponding band, then the correlation between $Y^{(1)}$ and $\hat{Y}^{(l)}$ is calculated as:

$$Q\left(A^l,\hat{A}^l\right) = \frac{\sigma_{A^l\hat{A}^l}}{\sigma_{A^l}\sigma_{\hat{A}^l}}\frac{2\mu_{A^l}\mu_{\hat{A}^l}}{\mu_{A^l}^2 + \mu_{\widehat{A^l}}^2}\frac{2\sigma_{A^l}\sigma_{\hat{A}^l}}{\sigma_{A^l}^2 + \sigma_{\widehat{A^l}}^2} \tag{6}$$

where μ_{A1} and $\mu_{\hat{A}^l}$ denote the mean vectors, σ_{A1} and $\sigma_{\hat{A}^l}$ denote the variances and $\sigma_{A^l\hat{A}^l}$ is the covariance of both images, respectively. The UIQI measure the average correlation Q over all the bands as follows,

$$\mathrm{UIQI}\left(A^l,\hat{A}^l\right)=\frac{1}{\lambda_h}\sum_{1}^{\lambda_h}Q\left(A^l,\hat{A}^l\right) \tag{7}$$

The UIQI values range from [−1, 1]. When both images are similar, $A=\hat{A}$, then the val of [UIQI+] = 1. For the final result, computed the overall UIQI of the estimated HSI by averaging the UIQI value of all bands.[16]

Proposed model design

In this proposed model, we explore the spatial and spectral quality of hyperspectral images by considering the sparsity and smoothness constraints in the spatial domain as well as the MV constraint to the simplex formed from the endmembers of the spectral domain. These constraints help us to attain a narrow solution space to the NMF problem. The $L_{1/2}$ regularisation, which shows superiority while considering the zero values when compared to other L-norms. Therefore, we incorporate the $L_{1/2}$-norm regularisation to enforce sparsity of abundance and total variation regularisation (TVR) to preserve the spatial smoothness of the model. The robust non-negative matrix factorisation (r-NMF) algorithm[18] is applied to describe the outlier residual term that captures the non-linear effects in the image. In this paper, the NMF-based unmixing algorithm uses the multiplicative update algorithm to update the basic terms and use β-divergence which minimises the objective function of NMF at each iteration until it reaches the pre-determined ε (epsilon) value.[7]

Linear mixing model (LMM)

Hongwei Han *et al.*[1] proposed a conventional LMM for HU. This LMM only assumes the macroscopic level of information about the pixel in the image. The LMM model considers only the reflecting endmembers present within a pixel. Therefore, LMM first estimates the endmember based on the scene of interest, then decomposes the input matrix into pure spectral signature and their fractional abundance corresponding to the estimated endmember.[19] LMM-based unmixing is shown in Figure 1.

Let the observed hyperspectral image be $\mathbf{Y}=[y_1,\ldots,y_k,\ldots,y_N]\in\mathbb{R}^{L\times N}$ with L bands and N pixels, then assume that p is the number of endmembers to be estimated. The endmember matrix is represented as $\mathbf{E}=[e_1,\ldots,e_p]\in\mathbb{R}^{L\times N}$ and its corresponding abundance matrix is represented as $\mathbf{A}=[a_1,\ldots,a_k,\ldots,a_N]\in\mathbb{R}^{p\times N}$. The matrix $\mathbf{R}=[r_1,\ldots,r_k,\ldots,r_N]\in\mathbb{R}^{L\times N}$ is the corresponding residual matrix that commonly assumed as some noise and other residual errors. Generally, in most existing literature this term $\mathbf{R}$ is considered as zero or close to zero.

With these notations, the LMM can be modelled based on pixel-wise $y_k\in\mathbb{R}^{L\times 1}$, as:

$$y_k=\mathbf{E}a_k+r_k, \tag{8}$$

The matrices representation of Figure 1 can be presented as:

$$\mathbf{Y}=\mathbf{EA}+\mathbf{R} \tag{9}$$

The LMM-based unmixing approaches are generally divided into geometrical and statistical. The geometrical-based unmixing approach includes two steps, first, extract the endmembers (spectral signature) and then estimate the abundances for the extracted endmembers. The common methods used for endmember extraction are pixel purity index (PPI), NFINDR, vertex component

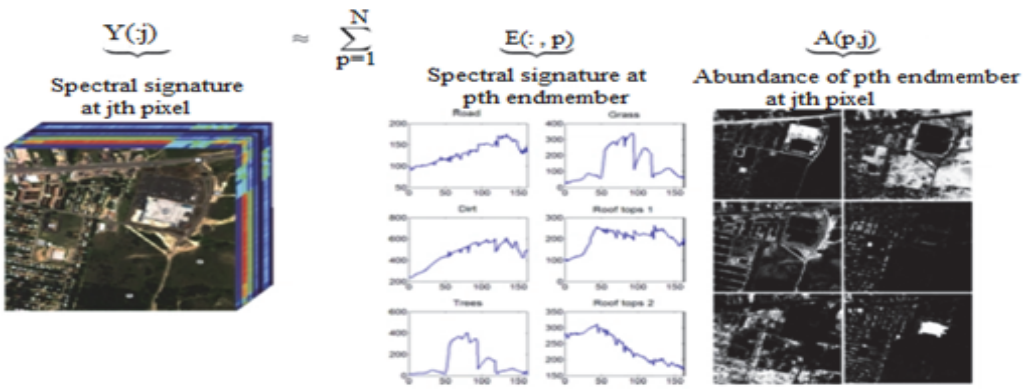

Figure 1. Linear SU of ground truth image.

analysis (VCA), simplex growing algorithm (SGA) and automated target generation process (ATGP). After the endmember extraction, abundances must be estimated for extracted endmember by using the partially or fully constrained least square method. These algorithms indicate that in the geometrical approach, the abundance estimation strongly depends on the performance of the endmember extraction.[20]

In a statistical-based unmixing algorithm, both endmembers and their abundances are estimated simultaneously without any purest pixel assumption. Independent component analysis (ICA) and NMF are typical statistical-based unmixing algorithms. ICA is a blind source unmixing method that does not satisfy the sum-to one constraint (ASC) mandatory for LMM. In contrast, NMF factorises the high-dimensional data into two non-negative matrices simultaneously without pure pixel assumption by satisfying both ASC and ANC. Moreover, the non-negativity (ANC) constraints must satisfy in NMF by default. Therefore, HU can be formulated well in NMF-based statistical approaches.[21]

Non-negative matrix factorisation (NMF)

NMF factorises a non-negative input matrix $\mathbf{Y}$ into two non-negative matrices namely endmember matrix $\mathbf{E}$ and abundance matrix $\mathbf{A}$. In the initialisation step, set the number of endmember p for the input matrix $\mathbf{Y} \in \mathbb{R}^{L \times N}$ and then calculate the initial endmember matrix $\mathbf{E} \in \mathbb{R}^{L \times p}$ by ATGP which is the most advanced endmember extraction method with purest pixel assumption. After the endmember estimation step, fractional abundance $\mathbf{A} \in \mathbb{R}^{p \times N}$ corresponding to these endmembers is calculated. Finally, these initial abundances are estimated using the fully constrained least square (FCLS) method that satisfies both sum-to-one and non-negativity constraints.[22]

In general, the NMF method can be formulated as follows:

$$\mathbf{Y} \approx \mathbf{EA} \tag{10}$$

Equation (10) implies that the input matrix $\mathbf{Y}$ is decomposed into two non-negative matrices endmember $\mathbf{E}$ and abundance $\mathbf{A}$ simultaneously.

NMF-based unmixing minimises the difference between $\mathbf{Y}$ and $\mathbf{EA}$ by performing the matrix decomposition iteratively until it meets the convergence condition. A squared Frobenius norm or Euclidean distance-based cost function is commonly used to measure the minimum distance in a HU problem. Then, the minimum distance of Equation (10) can be written as follows:

$$\text{subject to,} \quad \mathbf{E},\mathbf{A} \geq 0 \tag{11}$$

where $\mathbf{E}$ and $\mathbf{A}$ are endmember and abundance with non-negative values and $\|\cdot\|_F^2$ represents the Frobenius norm to minimise the error during the unmixing process.[23]

Sun *et al.*[24] stated that NMF is a powerful tool for identifying the materials present in hyperspectral images. Therefore, they concluded that NMF-based unmixing methods are consistent with the LMM. However, some minimum solutions exist in the solution space of NMF due to the non-convexity. So, adding constraints into an NMF model reduces the non-convexity problem, thereby obtaining an optimal solution to problems.[24]

NMF with outlier term

In general, the LMM method does not consider specific or localised areas of the image such as edges or boundaries of the heterogeneous regions. This property implies that LMM assumes only a limited number of pixels. Due to this limited number of pixels, the unmixing algorithms based on LMM find challenges to estimate endmembers and their abundance fractions accurately. From this premise, in a paper,[7] a new NMF-based LMM model was proposed, called r-NMF, for extracting endmember and abundance matrix by considering the localised portions of hyperspectral images. This r-NMF model decomposes the input matrix $\mathbf{Y}$ as follows,

$$\mathbf{Y} \approx \mathbf{EA} + \mathbf{R} \tag{12}$$

where $\mathbf{Y} \in \mathbb{R}^{L \times N}$ is an input matrix, $\mathbf{E}$, and $\mathbf{A}$ represents the endmember and the abundance matrix. $\mathbf{R}$ is an outlier term that accounts for the non-linearity effects such as residual noise, spectral and spatial variability. The approximation symbol (≈) in Equation (12) indicates the minimum dissimilarity measure between the input and factorised matrix. So, Equation (12) can be reformulated as:

$$\mathbf{D}(\mathbf{Y} \mid \mathbf{EA} + \mathbf{R}) \tag{13}$$

which is equal to

$$\mathbf{D}(\mathbf{Y} \mid \mathbf{EA} + \mathbf{R}) = [Z2] \tag{14}$$

then Equation (14) can be rewritten as

$$\min f(\mathbf{E},\mathbf{A},\mathbf{R}) = \mathbf{D}(\mathbf{Y} \mid \mathbf{EA} + \mathbf{R})$$

$$\text{subjected to, } \mathbf{E},\mathbf{A},\mathbf{R} \geq 0. \tag{15}$$

NMF with MV constraints

A significant geometrical constraint considered during the HU process is convex or simplex MV. This MV regulariser measures the simplex or convex hull

volume whose vertices are the endmembers selected for unmixing. This work proposes a centroid-based MV simplex. This method shrinks the volume of the simplex or convex hull by pulling the endmember (vertex of simplex) towards the centroid μ (centre of simplex).[25]

The NMF method with minimum volume-based constraints for Equation (15) can be represented as,

$$\min f(\mathbf{E},\mathbf{A},\mathbf{R}) = \mathbf{D}(\mathbf{Y} \mid \mathbf{EA}+\mathbf{R}) + \alpha\Phi_{MV}(\mathbf{E}) \tag{16}$$

$$\varnothing_{MV}(\mathrm{E}) = \sum_{i=1}^{p} e_i - \mu_2^2 \tag{17}$$

e centroid μ (centre of mass) of a simplex is estimated as follows:

$$\mu = \frac{1}{p}\sum_{i=1}^{p} e_i \tag{18}$$

where p denotes the number of endmembers and the e_i represents the mean value of each row in the endmember matrix **E**.

The MV-based NMF algorithm provides high-fidelity to the spectral signatures and thus helps to reduce the computational complexity in practical applications. Figure 2 shows the iterative process to represent the simplex with MV. In the $k+1^{th}$ iterative step, it selects a MV simplex for the hyperspectral image $\mathbf{Y}_h$.

NMF with sparsity constraints

The NMF method is non-convex in nature, so it is not easy to attain a globally optimal solution. Therefore, various constraints (or priors) are embedded into **E** and **A** to achieve the convexity on NMF. These constraints help to reduce the solution space and obtain a finite solution to the NMF algorithm.[2] A common constraint that is incorporated with the abundance matrix (**A**) is its sparsity. The abundance sparsity is an essential factor in hyperspectral image processing because the endmember distribution in each pixel does not fill in the whole scene of abundance map.[17] That means, each mixed pixel in an hyperspectral image contains only a few endmembers to represent the abundance matrix and many values should be zero or sparse, as shown in Figure 3.

While imposing the sparsity constraint on **A**, Equation (15) can be named as the sparse-NMF, which takes the following form:

$$\min f(\mathbf{E},\mathbf{A},\mathbf{R}) = \mathbf{D}(\mathbf{Y} \mid \mathbf{EA}+\mathbf{R}) + \alpha\Phi_{MV}(\mathbf{E}) + \beta\Phi_{spa}(\mathbf{A}) \tag{19}$$

$$\Phi_{spa}(\mathbf{A}) = \mathbf{A}_1 \tag{20}$$

where α· is a regularisation term that controls the sparsity measure function Φ(·) of the abundance matrix **A**.

NMF with $L_{1/2}$ regulariser

L-Norm regularisation methods are usually used to provide an optimal solution to the objective function.

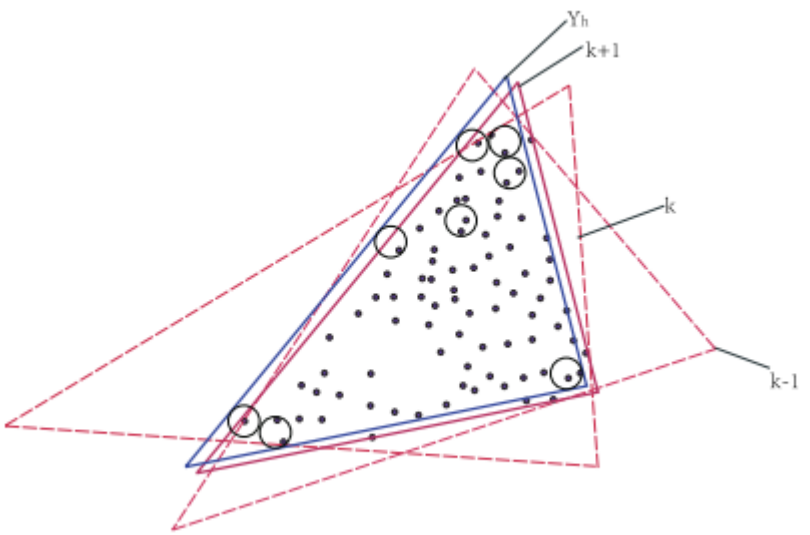

Figure 2. An iterative representation of MV simplex.

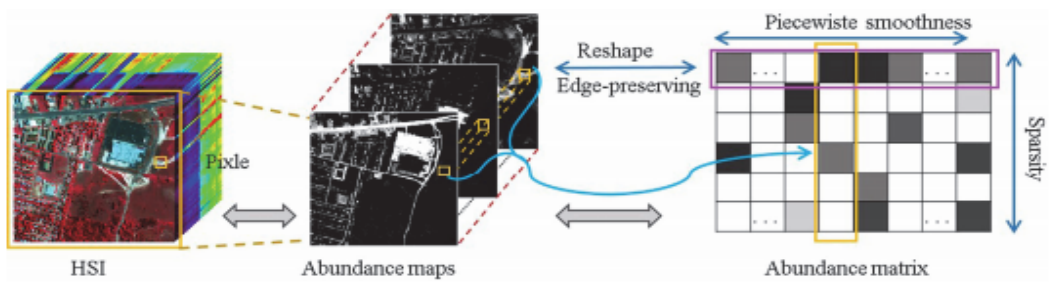

Figure 3. Representation of sparsity and smoothness constraints of the abundance matrix.

Many forms of regularisers are available to encourage the solution of the objective function. For example, the L_0 regulariser considers the zero or null elements in an abundance matrix and imposes the sparsest in the given cost function. However, the L_0 regulariser provides a non-deterministic polynomial-time hardness (NP-hard) optimisation solution. So, it is not easy to solve and take a final decision in real life. The L_1 regulariser is one of the most commonly used norms for considering the sparsity of the abundance matrix. Another popular L_2 regulariser generates smoothness but does not provide sparse results. Therefore, the L_1 regulariser is the effective method for obtaining sparse results, but it considers only a small sample size from high-dimensional data, and, therefore, only a subset of spectral signatures can be processed at a time. Due to these reasons, fractional regularisers L_q $(0 < q < 1)$ have been proposed and evaluated in the literature.[26]

Qian *et al.*[2] added $L_{1/2}$ regularisation to the NMF method named $L_{1/2}$-NMF. So, this method provides sparse-based unmixing and yields a more accurate estimation of abundance. Therefore, the $L_{1/2}$-NMF method is more effective for achieving better sparsity on the abundance matrix. Further, this $L_{1/2}$ regulariser also yields a more secure solution than the L_0 regulariser. From Equation (19), the $L_{1/2}$-NMF with sparsity regularisation model for unmixing can be formulated as:

$$\min f(\mathbf{E},\mathbf{A},\mathbf{R}) = \mathbf{D}(\mathbf{Y}\,|\,\mathbf{EA}+\mathbf{R}) + \alpha\Phi_{MV}(\mathbf{E}) + \beta\Phi_{spa}(\mathbf{A}) \quad (21)$$

$$\text{where } \Phi_{spa}(\mathbf{A}) = \mathbf{A}_{1/2} \quad (22)$$

Then Equation (22) is substituted in Equation (19) as follows,

$$\min f(\mathbf{E},\mathbf{A},\mathbf{R}) = \mathbf{D}(\mathbf{Y}\,|\,\mathbf{EA}+\mathbf{R}) + \alpha\Phi_{MV}(\mathbf{E}) + \mathbf{A}_{1/2} \quad \text{subjected to } \mathbf{E} \geq 0,\ \mathbf{A} \geq 0 \quad (23)$$

where

$$A_{1/2} = \sum_{i,j=1}^{p,N} a_{i,j}^{1/2} \quad (24)$$

and a_{ij} is the abundance value of the ith endmember at the jth pixel in the image.

Thus $L_{1/2}$-NMF with sparse constraint algorithm has better performance on HU. However, the $L_{1/2}$-NMF is less stable and highly sensitive to noise during the unmixing process, like other sparse-based NMFs. But we can improve the stability of this sparse constraint NMF algorithm by considering the structure information of the image. The structural similarity can be calculated with β-divergence as explained below.[26]

Total variation (TV) regulariser

The TV regulariser is another popular constraint that provides piecewise smoothness to the image by preserving the edge information. Furthermore, the use of the TV regularisation term also provides the ability to recover the image discontinuities. Therefore, this parameter plays a critical role in the image denoising process.[27]

In a hyperspectral image, each endmember pixel consists of a corresponding fractional abundance value represented in band-by-band form, as shown in Figure 4. These fractional abundance values of the same endmember correlate with each other to form the neighbouring pixels. This type of correlation among the neighbouring pixels provides smoothness to the image, because the neighbouring pixels in the abundance map of the same endmember should be almost similar. But sometimes, a sudden change may occur between adjacent pixel values. This sudden change mainly happens at the object boundary or the edges of the surface. Therefore, a TV regularisation constraint is added to our objective function to control such a sharp change and provide a piecewise smoothness on the abundance by preserving the spatial edge information. By considering this prior information in the hyperspectral images, we can effectively improve the accuracy of unmixing process.[10]

In general, the TV of abundance vector **A** can be expressed as,

$$\min_{\mathbf{A}} \mathrm{TV}(\mathbf{A}) \quad (25)$$

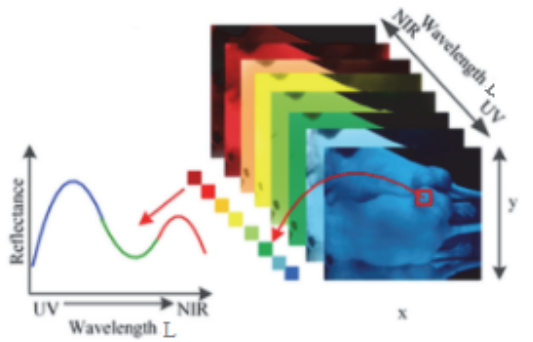

Figure 4. The smoothness of the mixed pixel in hyperspectral image.

where

$$TV(A) = H_h\tilde{A}_1 + H_v\tilde{A}_1 \tag{26}$$

Let i and j be the collection of adjacent pixels in the horizontal and vertical direction of the hyperspectral image, and then the TV function can be calculated as the differences between the adjacent pixels in abundance map $\mathbf{A}$ in both horizontal and vertical directions. This difference can be computed as follows:

$$H_h\tilde{A} = x_{ij} - x_{(i-1)j} \tag{27}$$

$$H_v\tilde{A} = x_{ij} - x_{i(j-1)} \tag{28}$$

By incorporating TV regularisation into Equation (23), the objective function of our proposed model becomes:

$$\min f(\mathbf{E},\mathbf{A},\mathbf{R}) = D(\mathbf{Y} \mid \mathbf{EA} + \mathbf{R}) + \alpha\Phi_{MV}(\mathbf{E}) + \beta\Phi_{spa}(\mathbf{A}) + \lambda\Phi_{TV}(\mathbf{A})$$

$$\text{subjected to } \mathbf{E},\mathbf{A},\mathbf{R} \geq 0 \tag{29}$$

Hence, the convex unmixing optimisation solution was obtained by imposing MV, sparsity, smoothness priors and non-linearity effects.

β-Divergence

The β-divergence is used to determine the performance degradation of an algorithm. This is done by measuring the difference between the referenced and estimated image. This function uses a single parameter β that takes values like 2, 1, 0.

β = 2: squared Euclidean distance (SED)
β = 1: Kullback–Leibler divergence (KLD)
β = 0: Itakura–Saito divergence (ISD)

The primary motivation for finding the β-divergence is to develop highly robust algorithms. Therefore, this algorithm is used for clustering, feature extraction, classification and blind source separation.[28]

The SED and KLD are the most commonly used in NMF to measure the dissimilarity between the original and estimated image. On the other hand, SED is the more popular in HU to measure the range of similarities between two images.[28]

In general, the SED between any two points (x, y) in an n-dimensional space is measured by

$$\beta_{Euc}(x \mid y) = \frac{1}{2}\sum_{i=1}^{N}(x-y)^{\beta} \tag{30}$$

Here, β = 2 in SED and the value of this β-divergence is always greater than or equal to zero. The value is zero for identical or similar points and gives high values as the dissimilarities between two points increase. The β-divergence between the original and estimated image, $\mathbf{Y}$ and $\tilde{\mathbf{Y}}$, are measured at each iteration using Equation (30). If this measurement is zero or close to zero, it indicates higher similarity between both images.

Algorithm implementation

In this paper, we implemented an algorithm for hyperspectral image unmixing using the image's non-linearity effects by accounting for spatial and spectral quality of the hyperspectral image by imposing certain extrinsic and intrinsic constraints into the image using the $L_{1/2}$-norm. By incorporating all these extrinsic and intrinsic priors or constraints, our proposed model can be represented by the following objective function:

$$\min f(\mathbf{E},\mathbf{A},\mathbf{R}) = D(\mathbf{Y} \mid \mathbf{EA} + \mathbf{R}) + \alpha\Phi_{MV}(\mathbf{E}) + \beta\Phi_{spa}(\mathbf{A}) + \lambda\Phi_{TV}(\mathbf{A})$$

$$\text{subjected to } \mathbf{E},\mathbf{A},\mathbf{R} \geq 0 \tag{31}$$

The matrix $\mathbf{R}$ is an outlier function that accounts the non-linear effects such as residual noise and other anomalies due to spatial and spectral variability. The parameters α, β and λ are the controlling terms; α controls the simplex with MV, β measures the sparsity elements of the abundance and λ controls the TV regularisation to maintain the spatial smoothness of the image. Including the parameters explained above in Equation (31), the proposed method attains an optimum minimisation solution to the unmixing problem with high robustness to the signal-to-noise ratio. In each of the optimisation steps, both $\mathbf{E}$, $\mathbf{A}$ and $\mathbf{R}$ are alternately updated till the cost function reaches convergence. Many works in the literature have already proposed such algorithms to update and solve the NMF. Among them, multiplicative update (MU)

algorithms[29] are commonly used for the solution of NMF. Many variants of the NMF method make it easy for implementation and produces good approximation results.[30]

Following the MU rule for NMF proposed by Lee and Seung,[30] they derive update rules for **E** and **A** as follows:

$$e_{[ij]}^{t+1} \leftarrow e_{[ij]}^{t} \frac{((a^t)^T y)_{ij}}{\left((a^t)^T a^t e^t\right)_{[ij]}} \tag{32}$$

$$a_{[ij]}^{t+1} \leftarrow a_{[ij]}^{t} \frac{(y(a^{t+1})^T)_{[ij]}}{\left(a^t e^{t+1} (e^{t+1})^T\right)_{[ij]}} \tag{33}$$

$$r_{[ij]}^{t+1} \leftarrow r_{[ij]}^{t} \frac{y_{ij}}{a^t e^t} \tag{34}$$

where $y_{[ij]}$, $e_{[ij]}$, $a_{[ij]}$ and $r_{[ij]}$ represent the input image, endmember, abundance and outlier matrix at the i,j^{th} pixels. The current and previous iteration steps are denoted as $t+1$ and t, respectively. Thus, the matrix representation of the above update rule can be as follows:

$$\mathrm{E} \leftarrow \mathrm{E} \circ \frac{\mathrm{YA}^{\mathrm{T}}}{\mathrm{EAA}^{\mathrm{T}}} \tag{35}$$

$$\mathrm{A} \leftarrow \mathrm{A} \circ \frac{\mathrm{E}^{\mathrm{T}}\mathrm{Y}}{\mathrm{E}^{\mathrm{T}}\mathrm{EA}} \tag{36}$$

$$\mathrm{R} \leftarrow \mathrm{R} \circ \frac{\mathrm{Y}}{\mathrm{EA}} \tag{37}$$

The endmember matrix **E**, abundance matrix **A** and outlier matrix **R** are updated iteratively with this MU rule until it reaches the convergence condition. Here, the ^{T} indicates the transpose of the matrix. The convergence condition is measured as the change in the ratio of cost function f must be below the given threshold ε,

$$\left| \frac{\mathrm{f}^t - \mathrm{f}^{t+1}}{\mathrm{f}^t} \right| < \varepsilon \tag{38}$$

where t is an iteration index, we can set a maximum number of iterations as a stopping criterion for practical implementation. If the convergence condition comes within that maximum number, the algorithm reaches the minimum optimisation condition, otherwise the algorithm's execution continues until it reaches the predefined number of iterations and take it as the stopping criteria.

This algorithm updates each term (**E**, **A**, **R**) conditionally using the MU rule. The updated term is fixed during the updating process, and all other parameters use the current value obtained at the previous update. Thus, the updating process continuously iterated until the objective function decreased or reached the stopping criteria.

Update of the endmember

The MU rules are commonly used in the NMF method for endmember estimation and is represented in Equation (19) as:

$$\mathrm{E} \leftarrow \mathrm{E} \circ \frac{\mathrm{YA}^{\mathrm{T}}}{\mathrm{EAA}^{\mathrm{T}}} \tag{39}$$

In our method, we use multiplicative gradient descent,[31] one of the popular approaches for NMF with β-divergence. At first, follow the multiplicative gradient descent approach for local convergence and then follow the iterative block coordinate approach for global convergence of endmember estimation.

Update of the abundances

In general, the MU rule for abundance estimation is represented in Equation (22) as follows:

$$\mathrm{A} \leftarrow \mathrm{A} \circ \frac{\mathrm{E}^{\mathrm{T}}\mathrm{Y}}{\mathrm{E}^{\mathrm{T}}\mathrm{EA}} \tag{40}$$

Updating **A** is somewhat difficulty and time consuming compared to the updating process of **E** and **R**. While updating the abundance, it needs to satisfy both sum-to-one and non-negativity constraints. These constraints help to reduce image blurring and poor contrast due to the inadequate falling of light during the image acquisition stage. To attain a sum-to-one constraint on the abundances map, it must normalise the abundance vector to unity. Normalisation is a process that changes the range of pixel intensity values between 0 and 1. Therefore, the normalisation process ensures that each pixel in the image has the same range of data distribution. This re-scaling technique makes the image processing much faster and stable. In general, matrix normalisation is done by simply dividing each element in the matrix by its magnitude. For this approach, the abundance matrix **A** is replaced with a new variable **U** which is a non-negative abundance vector with $p \times N$ elements, and then set

$$a_{pn} = \frac{u_{pn}}{u_{pn}} \tag{41}$$

The objective function of Equation (31) is then changed into the new optimisation problem w.r.t Equation (41) as

$$\min_{\mathbf{U}} f(\mathbf{U}) = \mathbf{D}(y_{\mathrm{In}} \mid e_{lp}\tilde{u}_{pn}) \tag{42}$$

i.e.,

$$\min_{\mathbf{U}} f(\mathbf{U}) = \mathbf{D}(\mathbf{Y}|\mathbf{E}\left[\frac{u_1}{u_{11}},\ldots\ldots\ldots,\frac{u_n}{u_{n1}}\right])$$

subjected to $\mathbf{U} \geq 0$ (43)

where y_{ln} is a vector having l values, and n is the number of vectors in the image matrix $\mathbf{Y}_{L\times N}$. This vector is decomposed into two other vectors with p number of endmembers named as endmember vector e_{lp} and abundance vector $\tilde{u}_{pn}$. Thus, Equation (43) ensures the sum-to-one constraint to the fractional abundance. After that we have to ensure the non-negativity constraint. For that, we use the multiplicative gradient descent approach. The multiplicative gradient descent approach states that, it is equivalent to updating each parameter by multiplying its value at the previous iteration by the ratio of the negative and positive parts of the gradient of the cost function about that parameter.[20] Suppose there is a function f(θ) which should be minimised over θ. Then gradient descent using the multiplicative algorithm is equivalent to,

$$\theta \leftarrow \tilde{\theta}\frac{\nabla_{\theta}^{-}\mathbf{D}(\theta)}{\nabla_{\theta}^{+}\mathbf{D}(\theta)} \tag{44}$$

where θ and $\tilde{\theta}$ represents an updating parameter at the current and previous iteration of a cost function. This parameter θ is defined as difference between two non-negative functions, $\nabla_{\theta}\mathbf{D}(\theta) = \nabla_{\theta}^{+}\mathbf{D}(\theta) - \nabla_{\theta}^{-}\mathbf{D}(\theta)$. We put all the negative terms in the numerator $\nabla_{\theta}^{-}\mathbf{D}(\theta)$ and all the favourable terms in the denominator $\nabla_{\theta}^{+}\mathbf{D}(\theta)$.

Then simply rewrite Equation (44) w.r.t. $\mathbf{U}$ as

$$u_{pn} \leftarrow \tilde{u}_{pn}\frac{\nabla_{u_{pn}}^{-} f(\tilde{\mathbf{U}})}{\nabla_{u_{pn}}^{+} f(\tilde{\mathbf{U}})} \tag{45}$$

where $\tilde{u}_{pn}$ represents the value of the previous iterations of the algorithm. Equation (45) ensures non-negativity of the updated term, and thus our algorithm ensures both sum-to-one and non-negativity constraints. Based on the gradient descent criterion.[28] The above two non-negative functions $\nabla_{u_{pn}}^{+} f(\tilde{\mathbf{U}})$ and $\nabla_{u_{pn}}^{-} f(\tilde{\mathbf{U}})$ can be calculated as the first and second derivative of w.r.t. $\tilde{u}$, such that

$$\nabla_{u_{pn}}^{-} f(\tilde{\mathbf{U}}) = \sum_{l} e_{lp} y_l \tag{46}$$

$$\nabla_{u_{pn}}^{+} f(\tilde{\mathbf{U}}) = \sum_{l} e_{lp}\tilde{y}_l \tag{47}$$

Substitute (46) and (47) in Equation (45)

$$u_{pn} \leftarrow \tilde{u}_{pn}\frac{\sum_l e_{lp} y_l}{\sum_l e_{lp}\tilde{y}_l} \tag{48}$$

Denoting

$$\tilde{y}_{\mathrm{In}} = \sum_{l}\tilde{s}_{\mathrm{In}} = \sum_{l}(e_{lp}\tilde{u}_{pn}).$$

Thus, to ensure both sum-to-one and non-negativity constraints, the MU rule for abundance estimation in Equation (22) can be modified as follows

$$\mathbf{A} \leftarrow \mathbf{A}.\frac{\mathbf{E}^{\mathrm{T}}\ \mathbf{Y} + \tilde{\mathbf{S}}.\tilde{\mathbf{Y}}}{\mathbf{E}^{\mathrm{T}}.\tilde{\mathbf{Y}} + \tilde{\mathbf{S}}.\mathbf{Y}} \tag{49}$$

where $\tilde{\mathbf{Y}} = \widetilde{\mathbf{EA}}$. Experimenting on our algorithm shows that the value of this objective function decreases at each iteration and thus makes the convergence faster.[7] Then the normalised representation of abundance coefficient according to Equation (41) can be written as:

$$\mathbf{A} \leftarrow \frac{\mathbf{A}}{\mathbf{A}} \tag{50}$$

In mathematics, $\mathbf{A}$ represents the magnitude or trace of the matrix, which determines matrix characteristics. This magnitude is calculated by summing the diagonal element of a given matrix. Therefore, the abundance estimation equation can be represented as follows:

$$\mathbf{A} \leftarrow \mathbf{A}\ \mathrm{diag}\left[a_{11},\ldots\ldots\ldots,a_{p1}\right]^{-1} \tag{51}$$

Update the outlier term R

Updating $\mathbf{R}$, the data-fitting outlier term, by the current values of $\mathbf{E}$ and $\mathbf{A}$. Then, the minimisation problem can be represented as

$$\min_{\mathbf{R}} f(\mathbf{R}) = \mathbf{D}(\mathbf{Y}|\mathbf{EA} + \mathbf{R}) \quad \text{s. t. } \mathbf{R} \geq 0 \tag{52}$$

The data-fitting term $\mathbf{R}$ is also updated in the same way as we did in the endmember update step by using the MU rule and normalising the outlier data to reduce the reconstruction error. That returns an auxiliary function that optimises and leading to the following updates,

$$r_{\mathrm{In}} = \tilde{r}_{\mathrm{In}}\frac{y_{\mathrm{In}}}{\tilde{y}_{\mathrm{In}} + \lambda\frac{\tilde{r}_{\mathrm{In}}}{\tilde{r}_{\mathrm{In}}^{2}}} \tag{53}$$

The matrix implementation of Equation (53) above can be written as

$$\mathbf{R} \leftarrow \mathbf{R}.\left[\frac{\mathbf{Y}}{\tilde{\mathbf{Y}} + \lambda\, \mathbf{R}\, \mathrm{diag}\left[r_{11},\ldots\ldots,r_{11}\right]^{-1}}\right] \tag{54}$$

As it turns out, the terms endmember, abundance and outlier are implemented in matrix form and updated by Equations (19), (51) and (54). Equations (17), (24) and (26) calculate the simplex volume of the endmember, whereas Equations (24) and (26) calculate the sparsity and smoothness of the abundance matrix. The below algorithm, named the JEIp $L_{1/2}$-NMF algorithm, explains the overall procedure of our proposed model.

JEIp $L_{1/2}$-NMF algorithm

Y and $\tilde{\mathbf{Y}}$ represent the input and output images.
E is the endmember matrix, **A** the abundance matrix, **R** the outlier terms and ϵ is the threshold value.
MV is the minimum volume, spa represents the sparsity and TV the total variance constraints.

Input: an observed HSI data $\mathbf{Y} \in \mathbf{R}^{L \times N}$.
p is the number of endmembers.

Initialise:
E = ATGP(**Y**), **A** = FCLS(**E**) and **R** = (**Y** – **EA**).
S = **EA**

Repeat:
Step 1:
Estimate:

$$\phi_{\mathrm{MV}}(\mathrm{E}) = \sum_{i=1}^{p} e_i - \mu_2^2$$

$$\phi_{TV}(A)_{1/2} \cdot \phi_{TV} = H_h \tilde{A}_1 + H_v \tilde{A}_1$$

$$\phi_{spa}(A)_{1/2} = \sum_{\mathrm{i,j=1}}^{\mathrm{p,\,N}} \mathrm{a}_{\mathrm{i,j}}^{1/2}$$

$\mathbf{Y} = \mathbf{S} + \mathbf{R} + \varphi_{\mathrm{MV}}(\mathbf{E}) + \psi_{\mathrm{spa}}(\mathbf{A})_{1/2} + \psi_{\mathrm{TV}}(\mathbf{A})_{1/2}$
Step 2: Update **E** as

$$\mathrm{E} \leftarrow \mathrm{E}\ \mathrm{o}\frac{\mathrm{YA}^{\mathrm{T}}}{\mathrm{EAA}^{\mathrm{T}}}$$

$\tilde{\mathbf{Y}} = \mathbf{S} + \mathbf{R} + \varphi_{\mathrm{MV}}(\mathbf{E}) + \phi_{\mathrm{spa}}(\mathbf{A})_{1/2} + \phi_{\mathrm{TV}}(\mathbf{A})_{1/2}$
Step 3: Update **A** as $\mathbf{A} \leftarrow \mathbf{A}\ \mathrm{diag}\left[a_{11},\ldots\ldots\ldots,a_{p1}\right]^{-1}$.
$\tilde{\mathbf{Y}} = \mathbf{S} + \mathbf{R} + \varphi_{\mathrm{MV}}(\mathbf{E}) + \phi_{\mathrm{spa}}(\mathbf{A})_{1/2} + \phi_{\mathrm{TV}}(\mathbf{A})_{1/2}$
Step 4: Update **R** as

$$\mathbf{R} \leftarrow \mathbf{R}.\left[\frac{\mathrm{Y}}{\tilde{\mathrm{Y}} + \lambda \mathbf{R}\,\mathrm{diag}\left[r_{11},\ldots\ldots,r_{11}\right]^{-1}}\right]$$

$\tilde{\mathbf{Y}} = \mathbf{S} + \mathbf{R} + \varphi_{\mathrm{MV}}(\mathbf{E}) + \phi_{\mathrm{spa}}(\mathbf{A})_{1/2} + \phi_{\mathrm{TV}}(\mathbf{A})_{1/2}$
Step 5: Estimate β-divergence at each iteration as

$$\beta_{Euc}\left(\tilde{\mathrm{Y}}|\mathrm{Y}\right) = \frac{1}{2}\sum_{i=1}^{N}\left(\tilde{\mathrm{Y}} - \mathrm{Y}\right)^2$$

Until reaches the maximum number of iterations or

$$\left\|\tilde{\mathrm{Y}} - \mathrm{Y}\right\|_2^2 < \varepsilon$$

Output: **E** and **A**.

Results and discussion

The proposed JEIp $L_{1/2}$-NMF algorithm for hyperspectral image unmixing is implemented on four different public datasets explained above. Endmember extraction algorithm ATGP and inversion algorithm FCLS are used to extract the endmember and the abundance map of the images in the dataset. Figures 5 and 6 show the images of four datasets and their extracted endmembers. Similarly, Figures 7–10 depict the estimated abundance map of the four datasets.

Parameter analysis

There are three parameters (α, β and λ) used in our algorithm, in which α measures the MV of simplex, β measures the sparsity of the abundance matrix and λ provides a piecewise smoothness to the image. The parameter β gives the sparsity levels of the abundance data.

$$\hat{a} = \frac{1}{\sqrt{L}}\sum_{l}\frac{\sqrt{N} - A_{l1}\ /\ A_{l2}}{\sqrt{N} - 1} \tag{55}$$

where the abundance value A_l denotes the hyperspectral image at band *l* with *L* bands and *N* pixels.[11]

Experiment analysis

We conducted out experiments and evaluated the effects of three parameters α, β and λ on our JEIp $L_{1/2}$-NMF algorithm using the four different datasets. For parameter β, we used the value as {1e-5, 1e-4, 1e-3, 1e-2, 0.01, 0.05, 0.1, 0.15, 0.2, 0.25, 0.3, 0.35, 0.4} calculated from Equation (55). According to the comparative analysis of the existing literature study, the performance of the other two parameters α and λ are also computed for the same set of values of β.[9]

Result analysis

The results obtained on our proposed method with three different parameters α, β and λ are observed. We tested various combinations for β and λ parameters in the given

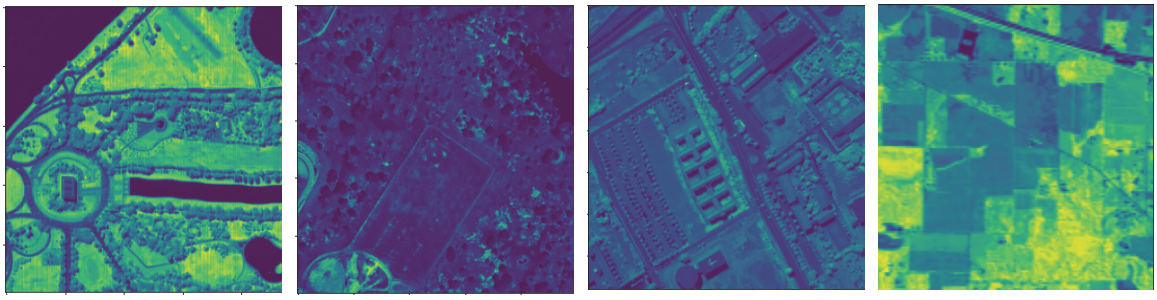

(a) (b) (c) (d)

Figure 5. The ground truth image of the four datasets (a) Washington DC Mall, (b) NEON, (c) Pavia University and (d) Indian Pines.

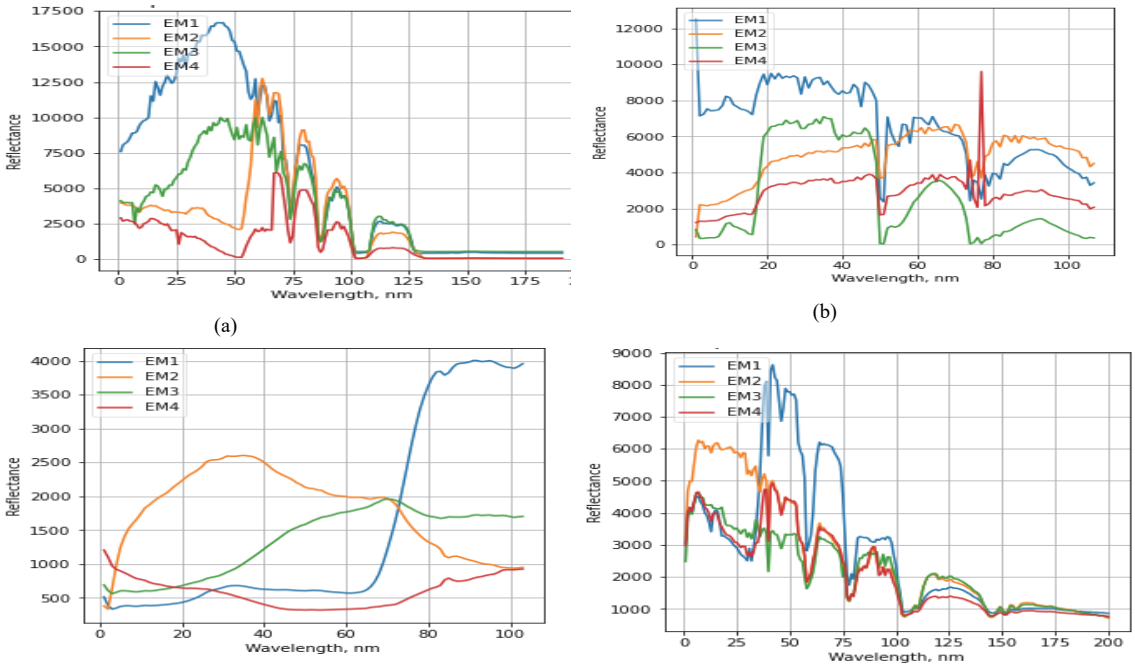

(a) (b) (c) (d)

Figure 6. The estimated endmembers of the four datasets. (a) Washington DC Mall, (b) NEON, (c) Pavia University and (d) Indian Pines.

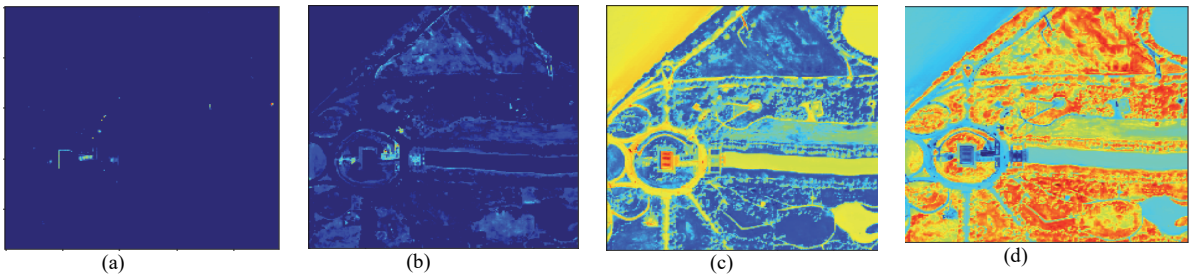

(a) (b) (c) (d)

Figure 7. Estimated abundance map of Washington DC dataset in our method. (a) Roof, (b) street, (c) grass and (d) tree.

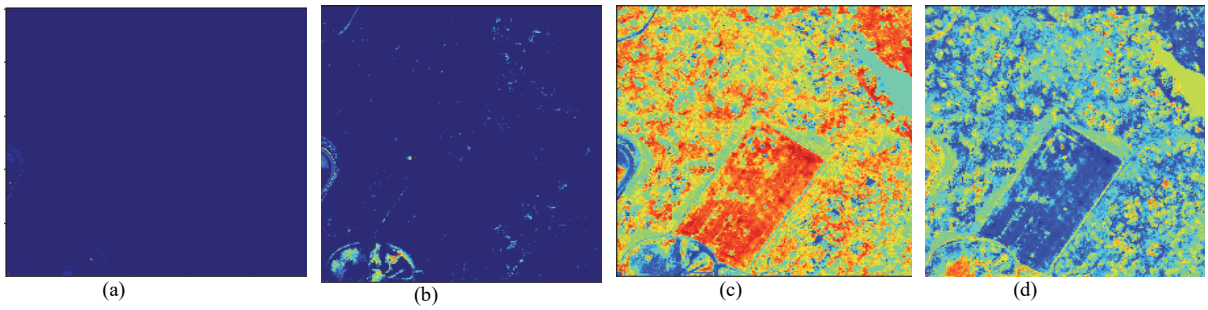

Figure 8. Estimated abundance map of NEON dataset in our method (a) water, (b) road, (c) soil and (d) vegetation.

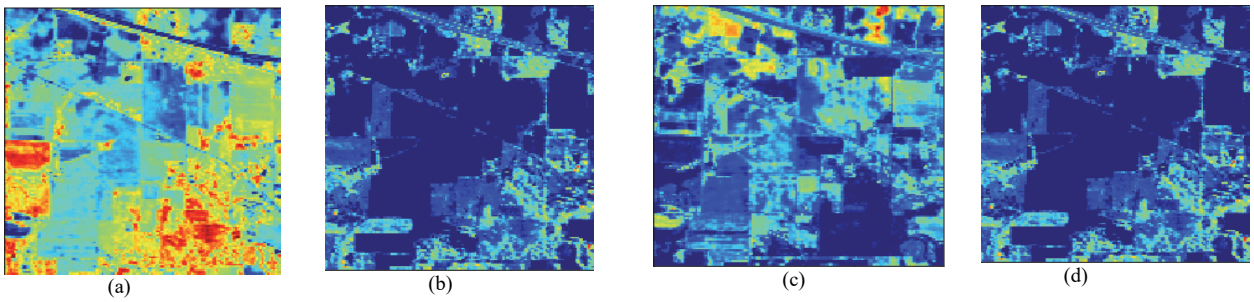

Figure 9. Estimated abundance map of Indian Pines dataset in our method (a) roof, (b) road, (c) vegetation and (d) water.

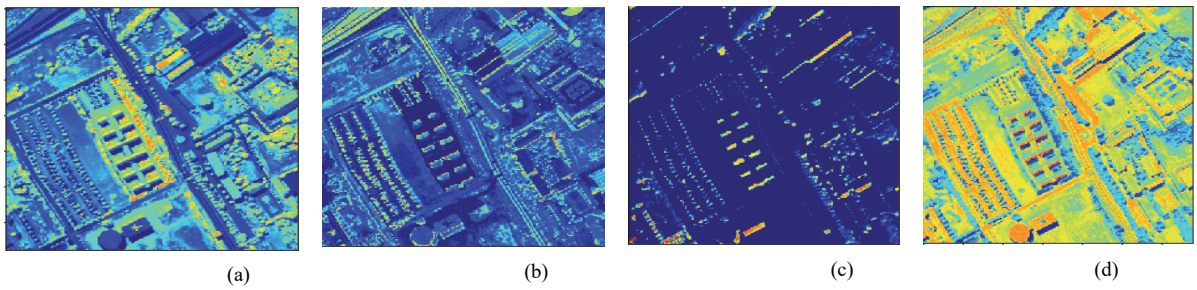

Figure 10. Estimated abundance map of NEON dataset in our method (a) roof, (b) road, (c) water and (d) vegetation.

range of values in four selected datasets. It shows that as and when the value of β and λ exceeds 0.0015, the value of SAM and RMSE increases rapidly. Similarly, when the values of parameters β and λ are below 0.0001, the RMSE value also starts rising. Therefore, the performance metrics provide better values between 0.0015 and 0.0001. Other performance measures such as SRE, PSNR and UIQI also show higher values in these ranges in all our four datasets. So, we set both β and λ = 0.00001 (1e-4) to achieve better performance. At the same time, the value of α at 1e-5 to 1e-3, both SAM and RMSE gives excellent and stable results. However, for all other values of α, both metrics show a rising tendency whether larger or smaller. Further, other performance measures for the same range of values also shows better results in our four datasets. Therefore, the optimal value of α should be in [1e-5, 1e-3]. Based on this analysis, we set all three parameters α, β and λ are 1e-4 in the rest of our experiments.

To evaluate the effectiveness of our algorithm, we also conducted experiments on our four hyperspectral datasets with the baseline unmixing methods and compared the results with the proposed method. We compared our HU methods with baseline unmixing methods includes original NMF, sparsity-based methods robust-NMF,[7] ICoNMF-TV,[8] Sparse-NMF[9] and MPEC-NMF.[11] Then, the performance of all these methods on our datasets is evaluated and

corresponding results obtained are shown in Table 1. Table 1 gives a comparative analysis of our proposed method with the various baseline methods using different quality measures. From this table, it is evident that the proposed JEIp $L_{1/2}$-NMF algorithm for hyperspectral image unmixing gives better performance in all the quality measures, such as SAM, RMSE, SRE, PSNR and UIQI, compared to the baseline unmixing approaches.

Dataset performance and discussion

The performance evaluation of our JEIp $L_{1/2}$-NMF algorithm for hyperspectral image unmixing is carried out on four different datasets by varying the number of endmembers. This comparison helps us to enhance the quality of our proposed algorithm. Initially, we compared the values of SAM and RMSE because it helps measure the quality of spectral and spatial data. The SAM and RMSE values on our JEIp $L_{1/2}$-NMF algorithm are represented in Figures 11 (a) and (b). This result shows that SAM gives a better value as the number of endmembers increases. That means by increasing the number of endmembers the quality of the estimated spectral data becomes good. On the other hand, the RMSE value gives smaller values as the number of endmembers rises to some extent up to five, after that, its value becomes higher. This indicates that increasing the number of endmembers up to five, our method gives high-quality spatial data. However, as it increases above five, the quality of the spatial data falls.

We also measured the value of SRE and PSNR for all our datasets in experiment by varying the number of endmembers, as shown in Figures 10(c) and (d). The PSNR shows better results on all the datasets with increasing number of endmembers whereas the SRE shows the worst value for the cases. To obtain both high-quality spectral and spatial data from the hyperspectral image, we compared the values of all four quality measures such as SAM, RMSE, PSNR and SRE. Finally, we concluded that unmixing the spectral image with endmembers less than five helps attain the best and good quality spectral and spatial data simultaneously without any distortion.

Conclusion

In this paper, we presented a non-negative matrix factorisation (NMF) based unmixing algorithm by adding some

Table 1. Performance measures of the HU algorithm used on different datasets with various quality measures.

Dataset	Method	NMF	r-NMF	ICoNMF-TV	Sparse-NMF	MPEC-NMF	Proposed
Washington DC Mall	SAM	1.31	1.30	1.75	1.17	1.14	**1.04**
	RMSE	1.62	1.24	2.06	1.47	1.40	**1.21**
	SRE	17.73	18.51	16.46	17.8	17.65	**18.85**
	PSNR	117.92	118.01	113.72	116.01	117.01	**118.32**
	UIQI	0.04	0.06	0.03	0.08	0.08	**0.12**
NEON	SAM	1.40	1.39	0.49	0.48	0.48	**0.47**
	RMSE	1.65	1.70	1.65	1.73	1.72	**1.35**
	SRE	18.35	18.23	18.32	17.88	17.81	**18.99**
	PSNR	115.66	115.38	115.68	115.23	115.23	**117.27**
	UIQI	0.030	0.026	0.012	0.021	0.026	**0.038**
Pavia University	SAM	0.021	0.029	0.021	0.019	0.017	**0.011**
	RMSE	3.93	6.12	4.71	3.92	4.31	**3.77**
	SRE	16.2	14.7	15.9	14.3	16.1	**16.4**
	PSNR	106.12	104.16	105.14	107.86	107.46	**108.46**
	UIQI	−0.12	−0.15	−0.13	−0.12	−0.18	**−0.11**
Indian Pines	SAM	0.31	0.33	0.30	0.29	0.29	**0.28**
	RMSE	1.10	1.09	1.15	1.68	1.67	**1.06**
	SRE	19.61	19.80	19.63	21.01	20.89	**21.21**
	PSNR	119.11	119.27	121.13	120.28	120.78	**121.77**
	UIQI	0.05	0.06	0.03	0.03	0.05	**0.07**

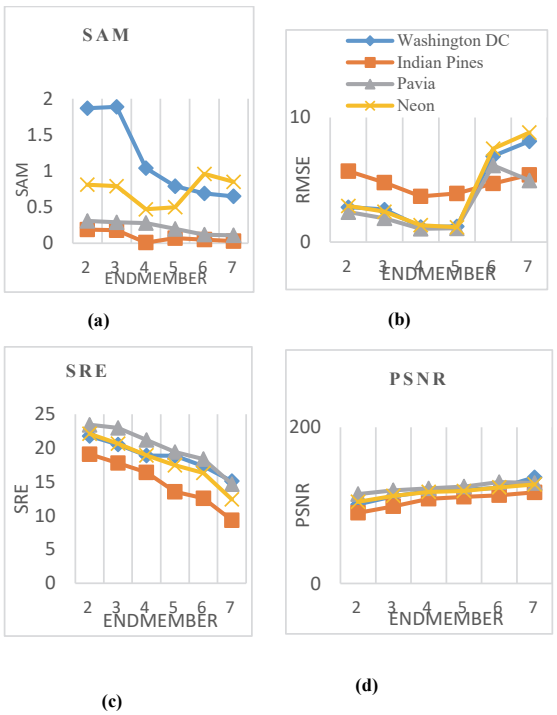

Figure 11. The performance of our method on four datasets by varying the endmembers. (a) SAM (b) RMSE, (c) SRE and (d) PSNR.

constraint parameters to enhance the quality of the images in spectral and spatial dimensions. This model is an extension of the standard linear mixing model (LMM) for considering the non-linear effects in the image by including an outlier residual term. These non-linear effects are treated as additive noise, sparse data or some spatial variations. This proposed hyperspectral image unmixing using the joint extrinsic and intrinsic priors with $L_{1/2}$-norms to non-negative matrix factorisation (JEIp $L_{1/2}$-NMF) algorithm updates each parameter by using a popular update method, called the MU rule which updates the endmember signatures, abundances and the outlier matrix iteratively until it reaches convergence. Initially, a TV regulariser term is added to the proposed algorithm to denoise the abundance maps, giving a smooth texture to the image. Then, the sparse regulariser term is included in the model that helps us to account for the zero values in the image. Therefore, sparsity is an effective tool for dimensionality reduction and that helps to use best endmember values of the pixels, thus the sparsity constraints increases the accuracy of the unmixing algorithm. Further, the abundance sparsity consideration is promoted by imposing the $L_{1/2}$ regulariser to the model. The proposed model also considered the structural information of the image at each iteration by using the β-divergence method. β-divergence determines the structural similarity between data more accurately during each decomposition of the hyperspectral image. This improves the decomposition performance and the estimated image is very consistent with the ground truth image. Finally, we used an epsilon value to prevent division by zero if the image has any zero-valued pixels. Epsilon stands for any arbitrary small number or pre-determined positive constants in image processing. This epsilon value is commonly used in certain conditions where the distance between the two elements can be made as small as any number that we wish to manage.

We experimented with our proposed unmixing method on four real-world datasets and analysed the performance of both spatial and spectral data by using various quality measures such as SAM, SRE, RMSE, PSNR and UIQI. Then we compared the effectiveness of our JEIp $L_{1/2}$-NMF algorithm with the baseline methods such as NMF, r-NMF, ICoNMF-TV, sparse-NMF and MPEC-NMF. From the results produced by all the above methods, the proposed algorithm gives better images with high-quality spatial and spectral dimensions and consumes less computational processing time than all the other methods. This work mainly focused on exploring spatial and spectral information by considering non-linear effects in the hyperspectral image. We can further improve the accuracy of unmixing performance by introducing more constraints or priors to the endmembers and abundance parameters of hyperspectral images.

References

1. H. Han, G. Wang, M. Wang, J. Miao, S. Guo, L. Chen, M. Zhang and K. Guo, "Hyperspectral unmixing via nonconvex sparse and low-rank constraint", *IEEE J. Select. Topics Appl. Earth Observ. Remote Sens.* **13,** 5704–5718 (2020). https://doi.org/10.1109/JSTARS.2020.3021520
2. Y. Qian, S. Jia, J. Zhou and A. Robles-Kelly, "Hyperspectral unmixing via $L_{1/2}$ sparsity-constrained nonnegative matrix factorization", *IEEE Trans. Geosci. Remote Sens.* **49(11),** 4280–4297 (2011). https://doi.org/10.1109/TGRS.2011.2144605
3. M.-D. Iordache, J.M. Bioucas-Dias and A. Plaza, "Collaborative sparse regression for hyperspectral unmixing", *IEEE Trans. Geosci. Remote Sens.* **52(1),** 341–354 (2014). https://doi.org/10.1109/TGRS.2013.2240001

4. F. Xiong, J. Zhou, J. Lu and Y. Qian, "Nonconvex nonseparable sparse nonnegative matrix factorization for hyperspectral unmixing", *IEEE J. Select. Topics Appl. Earth Observ. Remote Sens.* **13,** 6088–6100 (2020). https://doi.org/10.1109/JSTARS.2020.3028104
5. K. Qu, W. Bao and X. Shen, "Hyperspectral unmixing using weighted $L_{1/2}$ sparse total variation regularized and volume prior constrained nonnegative matrix factorization", *IGARSS 2019—2019 IEEE Int. Geosci. Remote Sens. Symp.* pp. 2147–2150 (2019). https://doi.org/10.1109/IGARSS.2019.8898830
6. L. Zhuang, C.-H. Lin, M.A.T. Figueiredo and J.M. Bioucas-Dias, "Regularization parameter selection in minimum volume hyperspectral unmixing", *IEEE Trans. Geosci. Remote Sens.* **57(12),** 9858–9877 (2019). https://doi.org/10.1109/TGRS.2019.2929776
7. C. Févotte and N. Dobigeon, "Nonlinear hyperspectral unmixing with robust nonnegative matrix factorization", *IEEE Trans. Image Process.* **24(12),** 4810–4819 (2015). https://doi.org/10.1109/TIP.2015.2468177
8. Y. Yuan, Z. Zhang and Q. Wang, "Improved collaborative non-negative matrix factorization and total variation for hyperspectral unmixing", *IEEE J. Select. Topics Appl. Earth Observ. Remote Sens.* **13,** 998–1010 (2020). https://doi.org/10.1109/JSTARS.2020.2977399
9. L. Zhou, X. Zhang, J. Wang, X. Bai, L. Tong, L. Zhang, J. Zhou and E. Hancock, "Subspace structure regularized nonnegative matrix factorization for hyperspectral unmixing", *IEEE J. Select. Topics Appl. Earth Observ. Remote Sens.* **13,** 4257–4270 (2020). https://doi.org/10.1109/JSTARS.2020.3011257
10. W. He, H. Zhang and L. Zhang, "Total variation regularized reweighted sparse nonnegative matrix factorization for hyperspectral unmixing", *IEEE Trans. Geosci. Remote Sens.* **55(7),** 3909–3921 (2017). https://doi.org/10.1109/TGRS.2017.2683719
11. K. Qu and W. Bao, "Multiple-priors ensemble constrained nonnegative matrix factorization for spectral unmixing", *IEEE J. Select. Topics Appl. Earth Observ. Remote Sens.* **13,** 963–975 (2020). https://doi.org/10.1109/JSTARS.2020.2976602
12. L. Tong, J. Zhou, B. Qian, J. Yu and C. Xiao, "Adaptive graph regularized multilayer nonnegative matrix factorization for hyperspectral unmixing", *IEEE J. Select. Topics Appl. Earth Observ. Remote Sens.* **13,** 434–447 (2020). https://doi.org/10.1109/JSTARS.2019.2963749
13. https://www.neonscience.org/resources/research-support (May 2019).
14. http://lesun.weebly.com/hyperspectral-data-set.html
15. N. Yokoya, C. Grohnfeldt and J. Chanussot, "Hyperspectral and multispectral data fusion, a comparative review of the recent literature", *IEEE Geosci. Remote Sens.* **5(2),** 29–56 (2017). https://doi.org/10.1109/MGRS.2016.2637824
16. Y. Zhou, L. Feng, C. Hou and S.-Y. Kung, "Hyperspectral and multispectral image fusion based on local low rank and coupled spectral unmixing", *IEEE Trans. Geosci. Remote Sens.* **55(10),** 5997–6009 (2017). https://doi.org/10.1109/TGRS.2017.2718728
17. P. Mhangara, W. Mapurisa and N. Mudau, "Comparison of image fusion techniques using Satellite Pour l'Observation de la Terre (SPOT) 6 satellite imagery", *Appl. Sci.* **10(5),** 1801 (2020). https://doi.org/10.3390/app10051881
18. M.E. Winter, "N-FINDR: an algorithm for fast autonomous spectral end-member determination in hyperspectral data", *Proc. SPIE Imaging Spectrometry V* **3633,** 266–275 (1999). https://doi.org/10.1117/12.366289
19. S. Prasad, J. Chanussot, J.E. Fowler, J. Bioucas-Dias and C.D. Creusere, "Introduction to the issue on Advances in Hyperspectral Data Processing and Analysis", *IEEE J. Select. Top. Signal Process.* **9(6),** 961–963 (2015). https://doi.org/10.1109/JSTSP.2015.2457631
20. S. Wang, N. Wang, D. Tao, L. Zhang and B. Du, "A K-L divergence constrained sparse NMF for hyperspectral signal unmixing", *IEEE International Conference and Security, Pattern Analysis, Cybernetics (SPAC)*, Wuhan, China, pp. 223–228 (2014).
21. H.-C. Li, S. Liu, X.-R. Feng and S.-Q. Zhang, "Sparsity-constrained coupled nonnegative matrix-tensor factorization for hyperspectral unmixing", *IEEE J. Select. Top. Appl. Earth Observ. Remote Sens.* **13,** 5061–5073 (2020). https://doi.org/10.1109/JSTARS.2020.3019706
22. J. Cao, L. Zhuo and H. Tao, "An endmember initialization scheme for nonnegative matrix factorization and its application in hyperspectral unmixing", *ISPRS Int. J. Geo-Inf.* **7(5),** 195 (2018). https://doi.org/10.3390/ijgi7050195

23. *Frobenius Norm*. Wolfram MathWorld. https://mathworld.wolfram.com/FrobeniusNorm.html
24. L. Sun, C. Han and Z. Liu, "Active set type algorithms for nonnegative matrix factorization in hyperspectral unmixing", *Computational Intelligence in Image Processing 2020* 9609302 (2019). https://doi.org/10.1155/2019/9609302
25. F. Yang, Z. Ping, F. Ma and Y. Wang, "Fusion of hyperspectral and multispectral images with sparse and proximal regularization", *IEEE Access* **7,** 186352–186363 (2019). https://doi.org/10.1109/ACCESS.2019.2961240
26. F. Xiong, J. Zhou, J. Lu and Y. Qian, "Nonconvex nonseparable sparse nonnegative matrix factorization for hyperspectral unmixing", *IEEE J. Select. Top. Appl. Earth Observ. Remote Sens.* **13,** 6088–6100 (2020). https://doi.org/10.1109/JSTARS.2020.3028104
27. V. Caselles, A. Chambolle and M. Novaga, "Total variation in imaging", in *Handbook of Mathematical Methods in Imaging*, Ed by O. Scherzer. Springer, New York, NY, pp 1016–1057 (2011). https://doi.org/10.1007/978-0-387-92920-0_23
28. C. Févotte and J. Idier, "Algorithms for nonnegative matrix factorization with the β-divergence", *Neural Comput.* **23(9),** 2421–2456 (2011). https://doi.org/10.1162/NECO_a_00168
29. C. Févotte and N. Dobigeon, "Nonlinear hyperspectral unmixing with robust nonnegative matrix factorization", *IEEE Trans. Image Process.* **24(12),** 4810–4819 (2015). https://doi.org/10.1109/TIP.2015.2468177
30. D.D. Lee and H.S. Seung, "Algorithms for non-negative matrix factorization", in *Advances in Neural Information Processing Systems 13 (NIPS 2000)*. Denver (2001). https://papers.nips.cc/paper/2000/hash/f9d1152547c0bde01830b7e8bd60024c-Abstract.html
31. M. Nakano, H. Kameoka, J. Le Roux, Y. Kitano, N. Ono and S. Sagayama, "Convergence-guaranteed multiplicative algorithms for nonnegative matrix factorization with β-divergence", *2010 IEEE International Workshop on Machine Learning for Signal Processing*, 11576358 (2010). https://doi.org/10.1109/MLSP.2010.5589233